Kinetics, stoichiometry, morphology and current drive capabilities of Ir-based silicides

G. Larrieu, Emmanuel Dubois, X. Wallart, J. Katcki

Kinetics, stoichiometry, morphology, and current drive capabilities of Ir-based silicides

Cite as: J. Appl. Phys. **102**, 094504 (2007); https://doi.org/10.1063/1.2802564
Submitted: 04 September 2006 • Accepted: 05 September 2007 • Published Online: 02 November 2007

G. Larrieu, E. Dubois, X. Wallart, et al.

Kinetics, stoichiometry, morphology, and current drive capabilities of Ir-based silicides

G. Larrieu,[a] E. Dubois, and X. Wallart
Institut d'Electronique de Microélectronique et de Nanotechnologie, IEMN/ISEN UMR CNRS 8520, Avenue Poincaré, Cité Scientifique, 59652 Villeneuve d'Ascq Cedex, France

J. Katcki
Institute of Electron Technology, Al. Lotników 32/46, 02-668 Warsaw, Poland

(Received 4 September 2006; accepted 5 September 2007; published online 2 November 2007)

A detailed study of the formation of iridium silicide obtained by ultrahigh vacuum annealing and atmospheric rapid thermal processing is proposed using x-ray photoelectron spectroscopy (XPS), transmission electron microscopy (TEM), and electrical characterizations. Using XPS analysis, the stoichiometry of each silicide phase (IrSi, $IrSi_{1.6}$) is identified. A model based on the variation of the measured intensity of the Ir $4f$ spectra is used to obtain the kinetic coefficients of reaction of Ir silicidation (E_A=2.48 eV, D_0=9 cm^2/s). TEM cross sections indicate that the roughness of the silicide/silicon interface increases with temperature. Lastly, electrical characteristics are used to identify the optimum annealing temperature to obtain an iridium silicide contact with the lowest Schottky barrier height to holes. © *2007 American Institute of Physics*. [DOI: 10.1063/1.2802564]

I. INTRODUCTION

As complementary-metal-oxide-semiconductor (CMOS) technology is entering in the decananometer era, the contact resistance associated to the silicide/silicon interface is identified as one of the biggest challenges to solve in order to preserve current drive capabilities. In that context, source/drain (S/D) engineering takes an increasing importance in the development of leading edge CMOS generations because of the increasing impact of S/D series resistances on transistor performance.[1] As titanium showed limitations for the silicidation ($TiSi_2$) of narrow lines at the 250 nm technology node, cobalt silicide ($CoSi_2$) became the industrial standard in CMOS integration down to the 90 nm technology node.[2] Nickel silicide (NiSi) is now the most widely accepted alloy owing to improved characteristics in terms of layer uniformity and sheet resistance.[3] The interesting properties of metal silicides, directly related to their utility in silicon technology, include low sheet resistance, reduced specific contact resistance on highly doped silicon (S/D), and also thermal stability.[4] In order to further pursue downscaling of metal-oxide-semiconductor-field-effect transistors (MOSFETs) in the sub-32 nm range of gate lengths, devices[5] that hierarchically combine alternative materials such as metallic gate, high-K dielectric[6] as well architecture concepts such as multigated channel have been proposed. Considering that the aforementioned innovations, referred to as *technology performance boosters*, are expected to deliver a higher current drive at shallower junction depth and reduced silicide thickness, extremely severe constraints are placed on the junction and contact technologies. In order to address these challenges (i.e., low specific contact resistance, abrupt highly doped junction), one alternative is to operate on lowly doped silicon and to use silicide contacts that present a very low Schottky barrier to electrons and holes for n-type and p-type MOSFETs, respectively.[5,7] Pt-based silicides (low Φ_{bp}) and rare earth silicides such as $ErSi_2$ (low Φ_{bn}) are commonly used for that purpose.[8,9] Surprisingly, iridium silicide which is known to present the lowest barrier to holes[10] has not yet been considered for p-MOS device integration. In that context, one important step to evaluate iridium silicide as a possible candidate in CMOS technology inevitably requests a detailed knowledge of its stoichiometry and associated electrical properties. Many stoichiometric flavors of iridium silicide have been suggested in the literature.[11–16] Several studies have pointed that iridium silicidation involves three successive phases: first, the formation of the IrSi phase was observed at ambient temperature,[11] 400 °C,[12] 450 °C,[13] while another $IrSi_x$ silicide was observed at a temperature close to 600 °C. The stoichiometry of the last silicide phase is still subject to debate: x=1.5,[14] x=1.6,[11,15] or x=1.75.[12,16] Finally for activation temperatures close to 1000 °C, the formation of $IrSi_3$ was also reported.[12,16] In this paper, we propose a detailed study of the mechanisms of iridium silicidation using various annealing conditions such as ultrahigh vacuum (UHV) and rapid thermal annealing with a particular attention on the interface reaction at room temperature, on the stoichiometry of the silicide and on the optimum conditions to obtain the lowest specific contact resistance. A description of the sample preparation technique and of the measurement procedures is given in Sec. II. The kinetic of Ir silicide formation and the stoichiometry of Ir-based silicides are critically analyzed using x-ray photoelectron spectroscopy (XPS) in Sec. III. Section IV provides transmission electron microscopy (TEM) observations that consolidate chemical analysis. Finally, Sec. V proposes electrical measurements of Ir-based silicide contacts that identify the optimum phase and temperature window to obtain the lowest Schottky barrier height.

[a]Electronic mail: guilhem.larrieu@isen.iemn.univ-lille1.fr

II. PREPARATION TECHNIQUES AND EXPERIMENTAL PROCEDURES

A. XPS analysis

The samples have been analyzed by XPS, using a Physical Electronics 5600 spectrometer fitted in an UHV chamber (base pressure 1×10^{-10} Torr). We use a monochromatized Al x-ray source ($h\nu=1487$ eV) and the detection angle is 45° with respect to the sample surface normal. For depth profile analysis, we use an Ar+ ion gun with an ion energy of 1 keV and a beam raster of 5×5 mm^2. Concentration profiles are obtained using standard sensitivity factors provided by the manufacturer.[17]

B. Sample preparation

Samples consist of pieces cut from (100) Si bulk (p-type doped 4–10 Ω cm). For TEM cross sections, (100) silicon-on-insulator (SOI) wafers (p-type doped 4–10 Ω cm) with a 100 nm thick active silicon layer have been used to better evaluate the thickness of the silicide layer and the amount of consumed Si. A first degreasing step was performed in acetone followed by a rinse in isopropyl alcohol. A standard RCA cleaning step was subsequently applied to remove any possible surface contamination. Before being loaded into the vacuum deposition system, the surface oxide was removed by a dip in diluted fluorhydric acid (1%) for 30 s followed by a rinse in de-ionized water. Ir films were deposited by electron beam evaporation with a low deposition rate (0.1 Å/s) to keep the sample temperature below 40 °C. The base vacuum before deposition was 2×10^{-8} Torr. A gentle surface etch was realized *in situ* using Ar sputtering at 60 eV during 20 s. Unless otherwise specified in the following of this paper, silicidation steps at various temperatures were processed in a rapid thermal annealing (RTA) system under forming gas (N_2:H_2/95:5).

C. Electrical measurements

Standard techniques to characterize Schottky barrier height are not suitable when they are applied to very low barrier and weakly doped substrates.[18] The mechanisms of current injection involve a complex combination of the thermionic emission (TE) and field emission (FE).[18] Instead, an alternative method was used[18,19] to characterize the current drive capability of two Schottky contacts separated by a micrometer gap. Schottky barrier heights were determined using an extraction procedure that couples experimental data to a transport model that accounts for TE and FE as well as barrier lowering due to image charge induction.[18] The sheet resistance of the silicide layer is obtained using a conventional four-point probes technique.

III. XPS ANALYSIS

A. Kinetic of iridium formation under UHV annealing

1. Identification of the silicide phase

The kinetic of reaction leading to the formation of IrSi is a mechanism controlled by diffusion of the most mobile species through the incipient layer of silicide. Silicon is the major migrant species[12] and the expansion coefficient $[d(\mathrm{IrSi})/d(\mathrm{Ir})]$ is close to 2.[20] In the proposed experiments, the reaction of silicidation is controlled under ultrahigh vacuum (UHV) in the XPS chamber to enable real time analysis. The initial iridium overlayer is 10 nm thick and the temperature is varied between 20 and 600 °C in 120 min, corresponding to a ramp of 4.8 K/min. Only the top surface of the sample is analyzed during annealing in order to detect changes of surface composition over the electron escape depth (~3 nm). Figure 1(a) shows the variation of the iridium and silicon concentrations as a function of the annealing temperature, obtained from the Ir 4f and Si 2p emission lines, respectively. In order to determine exactly the temperature of complete conversion of metallic iridium in IrSi silicide, the chemical shift related to the binding energy of Ir 4f has been analyzed in detail. Figure 1(b) shows a selection of the Ir 4f spectra recorded during annealing. At 20 °C, the

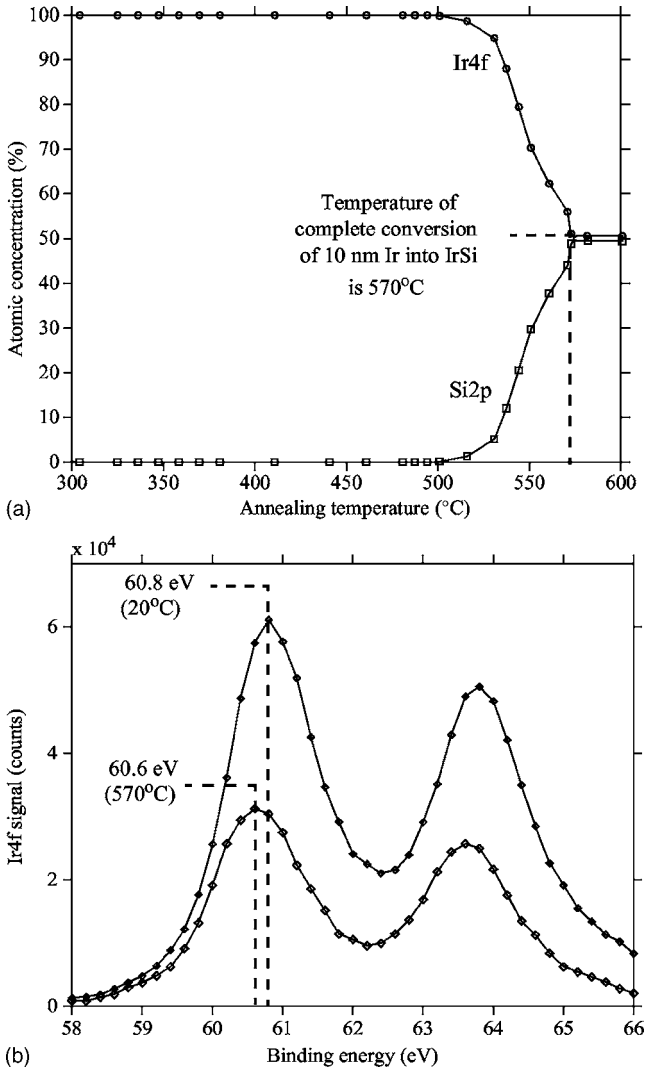

FIG. 1. Kinetics of IrSi silicidation reaction. A 10 nm Ir thick overlayer is annealed under ultrahigh vacuum using a constant temperature ramp (4.8 K/min) (a) Dependence of the atomic concentrations on the annealing temperature obtained from the Ir 4f and Si 2p XPS emission lines recorded from the top surface. The temperature for which the front of silicidation reaction reaches the top surface is 570 °C. (b) Ir 4f spectra recorded at specific temperatures, 20 and 570 °C, relevant to metallic Ir and IrSi, respectively.

position of the Ir $4f_{7/2}$ peak is centered at 60.8 eV, which corresponds to the binding energy of metallic iridium.[21] The peak position remains unchanged up to 500 °C and shifts to a weaker binding energy indicating that the front of reaction has progressed towards the surface within the depth of analysis. At 570 °C, the peak is centered at a binding energy of 60.6 eV, revealing the complete conversion of metallic Ir into silicide. The phase of iridium silicide is clearly identified as being IrSi [Fig. 1(a)]. On the other hand, it is worth noting that the Si $2p$ emission line exhibits a chemical shift of 0.6 eV, from 99.2 eV (Si–Si) to 99.8 eV (Ir–Si), related to the formation of Ir–Si bonds. To identify the kinetic coefficients of the IrSi formation reaction, a similar experiment has been conducted using a 3 nm thick iridium layer. Since the iridium overlayer lies within the depth of XPS analysis, the variation of composition can be detected at the very beginning of the reaction. The thermal budget was applied by varying the temperature from RT to 550 °C for 100 min, corresponding to an average ramp of 5.5 K/min. Figure 2(a) shows the atomic concentration of iridium and silicon as a function of the annealing temperature while Fig. 2(b) provides a selection of Ir $4f$ spectra recorded during the silicidation reaction. At 20 °C, the Ir $4f_{7/2}$ peak can be deconvolved in two contributions: a major one centered at 60.8 eV indicating that most of the layer is composed of metallic Ir and a secondary contribution centered at 60.6 eV revealing that the reaction of silicidation has already started at ambient temperature. At the beginning of the temperature ramp, the Ir $4f_{7/2}$ peak derives slowly to a binding energy of 60.6 eV as shown in Fig. 2(b) for a temperature of 500 °C. It subsequently recovers its initial position 60.8 eV at 550 °C. This shift in binding energy is attributed to the growth of another silicon-rich silicide phase at IrSi/Si interface when the formation of the IrSi layer is completed. Almendra *et al.*[22] showed that the three phases can coexist for a range of iridium thickness around several tens of nanometers. This point constitutes a considerable difference with platinum silicide for which the difference between the activation energies associated to Pt_2Si and PtSi is too large to observe this scenario. In the present experiment, the temperature of complete conversion of the iridium overlayer cannot be clearly identified because of the simultaneous presence of several phases. However, Fig. 2(a) strongly suggests that the interval of complete silicidation ranges between 450 and 530 °C.

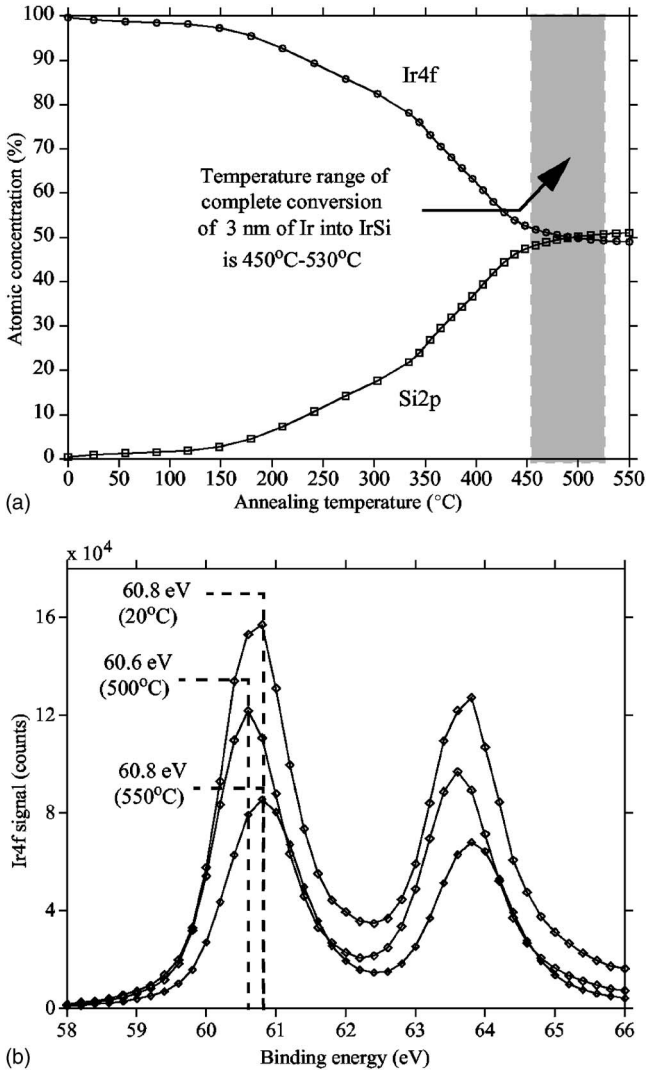

FIG. 2. Kinetics of IrSi silicidation reaction. A 3 nm Ir thick overlayer is annealed under ultrahigh vacuum with a constant temperature ramp (5.6 K/min). (a) Dependence of the atomic concentrations on the annealing temperature obtained from the Ir $4f$ and Si $2p$ XPS emission lines recorded from the top surface. The temperature for which the front of silicidation reaches the top surface lies between 450 and 530 °C. (b) Ir $4f$ spectra at specific temperatures, 20, 500, and 550 °C: at the beginning of the temperature ramp, the Ir $4f_{7/2}$ peak derives slowly to a binding energy of 60.6 eV for a temperature of 500 °C and subsequently recovers its initial position 60.8 eV at 550 °C attributed to the growth of another silicon-rich silicide phase at IrSi/Si interface when the formation of the IrSi layer is completed.

2. Kinetic coefficients of reaction

In order to obtain a more accurate determination of the temperature of complete transformation of the initial iridium layer, a model based on the variation of the measured intensity of the Ir $4f$ spectra has been used. The system can be schematized using a two-layer system, as shown by the inset in Fig. 3. The top layer of thickness y represents the remaining metallic iridium while the bottom layer of thickness x corresponds to the IrSi phase. For a 3 nm thick iridium layer, we can consider that the thickness of the third phase ($IrSi_x$) remains negligible when the entire metallic layer is converted into IrSi. As the silicidation reaction proceeds, the thickness x of the IrSi layer can be related to y, the thickness of the remaining Ir overlayer, using the following relationship:

$$y + x/\alpha = y_0, \tag{1}$$

where α is the expansion coefficient of IrSi phase, equal to ~2 and y_0 stands for the thickness of the metal overlayer equal to 3 nm. The intensity I_{Ir} associated to the iridium emission line can be decomposed into one contribution I_{Ir}^{y} coming from the iridium top layer and a second one I_{Ir}^{x} originating from the growing silicide layer,

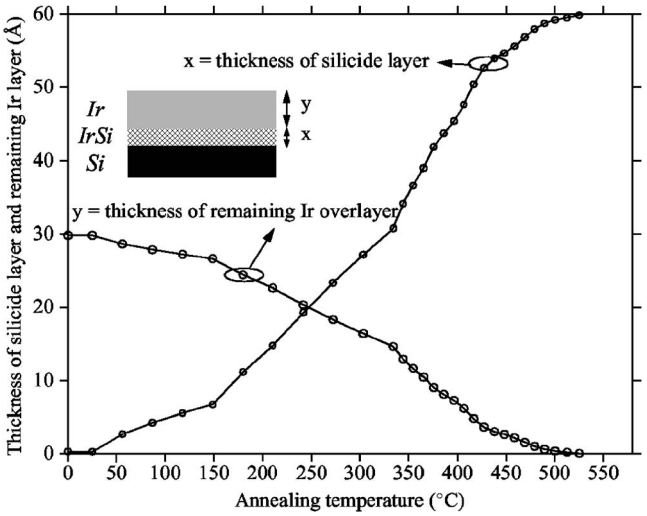

FIG. 3. Variations of the thickness of remaining Ir overlayer (x) and of the growing IrSi silicide layer (y) as a function of the annealing temperature (constant ramp of 5.6 K/min). Results are based on the analysis of the Ir $4f$ emission line. The temperature for which the front of reaction reaches the top surface is deduced to be 520 °C.

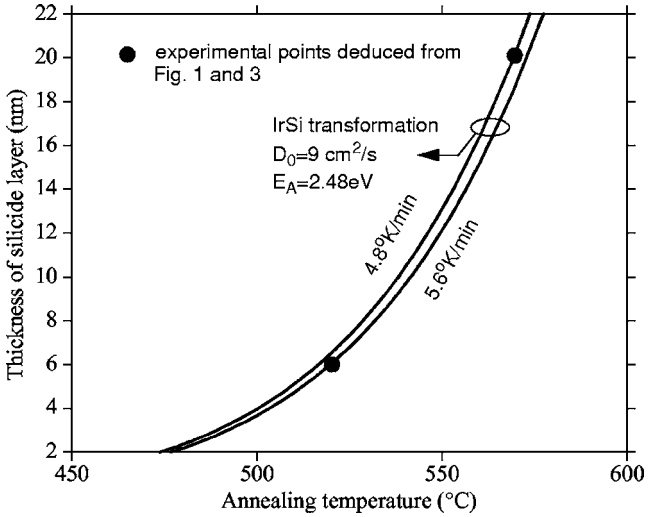

FIG. 4. Thickness of the IrSi layer as a function of the annealing temperature for two heating ramps (4.8 and 5.6 K/min). The preexponential diffusion coefficient D_0=9 cm^2/s and the activation energy E_A=2.48 eV are deduced from the best match of a classical parabolic growth rate equation to experimental data.

$$I_{\mathrm{Ir}}^{y} = N_{\mathrm{Ir}}^{y}\int_{0}^{y} e^{-y'/\lambda_{\mathrm{Ir}}^{y}\sin\theta}dy' = \lambda_{\mathrm{Ir}}^{y}\sin\theta N_{\mathrm{Ir}}^{y}(1-e^{-y/\lambda_{\mathrm{Ir}}^{y}\sin\theta}), \tag{2}$$

$$I_{\mathrm{Ir}}^{x} = N_{\mathrm{Ir}}^{x}\int_{y}^{x+y} e^{-x'/\lambda_{\mathrm{Ir}}^{x}\sin\theta}dx' = \lambda_{\mathrm{Ir}}^{x}\sin\theta N_{\mathrm{Ir}}^{x}e^{-y/\lambda_{\mathrm{Ir}}^{x}\sin\theta}(1-e^{-x/\lambda_{\mathrm{Ir}}^{x}\sin\theta}), \tag{3}$$

where N_{Ir}^{y} and N_{Ir}^{x} are the concentration of iridium in the top Ir and bottom IrSi layers, respectively. $\lambda_{\mathrm{Ir}}^{y}$ and $\lambda_{\mathrm{Ir}}^{x}$ stand for the electron escape depth corresponding to each material layer. Finally, θ denotes the detection takeoff angle. Assuming that the electron escape depth is the same in the Ir and IrSi layers, i.e., $\lambda_{\mathrm{Ir}}^{y}=\lambda_{\mathrm{Ir}}^{x}=\lambda_{\mathrm{Ir}}$, the total Ir $4f$ intensity can be expressed as

$$I_{\mathrm{Ir}} = I_{\mathrm{Ir}}^{\mathrm{ref}}\left[(1-e^{-y/\lambda_{\mathrm{Ir}}\sin\theta}) + \frac{N_{\mathrm{Ir}}^{x}}{N_{\mathrm{Ir}}^{y}}e^{-y/\lambda_{\mathrm{Ir}}\sin\theta}(1-e^{-x/\lambda_{\mathrm{Ir}}\sin\theta})\right], \tag{4}$$

where $I_{\mathrm{Ir}}^{\mathrm{ref}}=I_{\mathrm{Ir}}^{y}|_{y=\infty}=\lambda_{\mathrm{Ir}}\sin\theta N_{\mathrm{Ir}}^{y}$ represents the reference intensity of bulk metallic Ir. Accounting for the ratio of Ir stoichiometry $N_{\mathrm{Ir}}^{x}/N_{\mathrm{Ir}}^{y}=0.5$ and using $\alpha=2$, Eqs. (1) and (4) can be combined into a second order equation that finally yields

$$y = -\lambda_{\mathrm{Ir}}\sin\theta\ln\left[(1-I_{\mathrm{Ir}}/I_{\mathrm{Ir}}^{\mathrm{ref}}) + \sqrt{(I_{\mathrm{Ir}}/I_{\mathrm{Ir}}^{\mathrm{ref}}-1)^2-\exp\left(-\frac{2y_0}{\lambda_{\mathrm{Ir}}\sin\theta}\right)}\right]. \tag{5}$$

Based on Eq. (5), Fig. 3 presents the variations of y and x corresponding to the thickness of the Ir and IrSi layers as a function of the annealing temperature. Based on this result, the temperature of complete conversion of metallic iridium into silicide is deduced to occur at 520 °C. From the same experiment, it is also possible to estimate the kinetics coefficients of IrSi formation. Figure 4 represents the thickness variations of the IrSi layer as a function of the temperature, taking into account the differences in the heating rates, i.e., 5.6 K/min in the first experiment and 4.8 K/min in the second one. These curves were obtained using a classical growth rate equation associated to a diffusion mechanism given by

$$d_{\mathrm{IrSi}}^{2} = \int_{0}^{t} D dt = \int_{T_0}^{T} D(dT/dt) = D_0(dT/dt)^{-1}\frac{k_B}{E_A}\left[T^2\exp\left(-\frac{E_A}{k_BT}\right) - {T_0}^2\exp\left(-\frac{E_A}{k_BT_0}\right)\right], \tag{6}$$

where T is the temperature of complete silicidation, and E_A the activation energy coefficient. D and D_0 are the temperature dependent and preexponential diffusion coefficients, respectively. Finally, T_0 is the starting temperature set to 20 °C. An optimization procedure using a least-square method allowed the extraction of the activation energy E_A =2.48 eV and the preexponential diffusion coefficient D_0 =9 cm^2/s. The activation energy is 30% higher than that determined by Petersson *et al.*[12] This discrepancy can be explained by the thickness range considered in its experiment, several hundreds of nanometers, which introduces a modification of the kinetics of reaction probably related to the additional formation of the IrSi_x phase.[16]

B. Temperature dependence of Ir silicide formation

1. Iridium silicide at room temperature

Morgan *et al.* analyzed by XPS a 7 Å iridium layer deposited on a clean Si (100) surface without any temperature activation.[11] The shift in Ir $4f$ and Si $2p$ binding energies

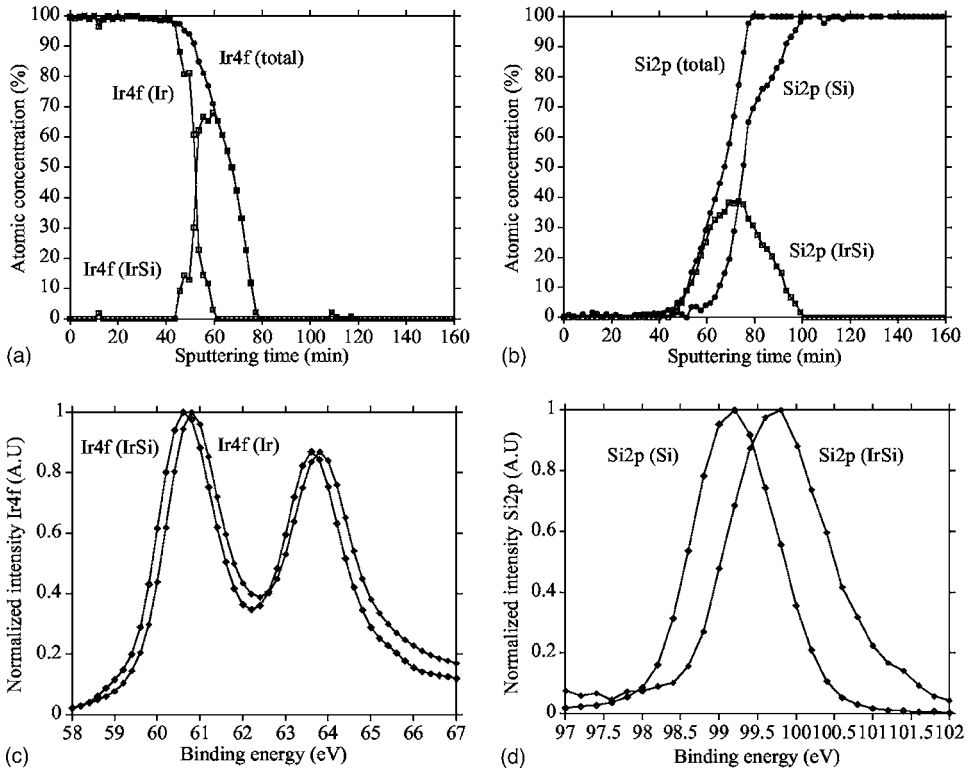

FIG. 5. XPS analysis of the initial Ir-silicide reaction occurring at room temperature: (a) Ir 4*f* depth profile deconvolved into its Ir 4*f* (IrSi) and Ir 4*f* (Ir) contributions. (b) Si 2*p* depth profile deconvolved into its Si 2*p* (IrSi) and Si 2*p* (Si) contributions. (c) Extracted basis of spectra used in the deconvolution of the Ir 4*f* profile shown in (a): 60.8 and 60.6 eV are relevant to metallic and IrSi-like binding energies. (d) Extracted basis of spectra used in the deconvolution of the Si 2*p* profile shown in (b): 99.2 and 99.8 eV are relevant of elemental silicon and IrSi-like binding energies.

revealed the presence of IrSi-like bonds. In the present contribution, a 15 nm thick iridium layer was deposited by e-gun evaporation and was directly analyzed without heat treatment to investigate the initial interface reaction. The XPS Ir 4*f* and Si 2*p* emission lines were recorded to determine the depth composition profiles during Ar sputtering. These original photoemission measurements have been fitted using a standard linear least-squares procedure to identify the chemical states of Ir and Si, respectively. Figure 5(a) shows the decomposition of the Ir 4*f* profile deconvolved in two contributions Ir 4*f* (IrSi) and Ir 4*f* (Ir). The reference spectra used to extract these two depth profiles are given in Fig. 5(c). The two Ir 4*f* spin-orbit doublets ($4f_{5/2}$,$4f_{7/2}$) exhibit a chemical shift of 0.2 eV from 60.8 to 60.6 eV corresponding to the activation of a silicidation reaction involving the formation IrSi film. This result is consolidated by Fig. 5(b) which gives the decomposition of the Si 2*p* profile in two components, Si 2*p* (IrSi) and Si 2*p* (Si). The reference basis of spectra used to obtain these deconvolved Si 2*p* profiles are provided in Fig. 5(d), indicating a chemical shift of Si 2*p* peak from 99.2 to 99.8 eV what is also attributed to chemical bonding between Ir and Si. The variations of Si 2*p* (IrSi) and Ir 4*f* (IrSi) profiles over a sputtering time window ranging from 30 to 60 min indicate that a silicidation reaction occurred at room temperature. However, it remains difficult to ascertain the exact composition of the incipient silicide layer all the more since the silicidation reaction is probably not regular but locally takes place in the form of patches.

2. Iridium silicide formation upon different RTA conditions

To complete our kinetic study of Ir silicidation, the impact of the activation temperature has been investigated when annealing is conducted at atmospheric pressure under forming gas (N_2:H_2/95:5). For that sake three distinct temperatures (300, 600, and 900 °C) have been considered for RTA activation during 2 min, starting from an iridium layer of 15 nm. Figure 6(a) gives the atomic composition depth profile obtained by XPS analysis for a sample annealed at 300 °C. For sputtering times between 48 and 55 min, the iridium and silicon concentrations clearly describe a plateau over which the 1:1 IrSi stoichiometry is verified, suggesting that metallic Ir is converted into IrSi silicide. This observation is consistent with the Si $2p_{3/2}$ and Ir $4f_{7/2}$ peaks centered at 99.8 and 60.6 eV, respectively, which are relevant to IrSi-like bonds. Figure 6(b) presents the atomic concentration depth profile obtained from the Si 2*p* and Ir 4*f* photoemission core levels for a 15 nm iridium overlayer annealed at 600 °C. This graph first reveals that the complete metallic iridium layer is converted into silicide. It also clearly appears that the first section over the first 35 min of sputtering is indicative of a stable stoichiometric IrSi composition. In the sputtering window covering the 35–40 min range, the Ir $4f_{7/2}$ peak centered at 60.6 eV shifts to higher energies indicating the growth of a more complex phase $IrSi_x$ between the IrSi layer and the Si substrate. From a quantitative standpoint, a careful inspection of Fig. 6(b) reveals the presence of narrow plateaus in the 40–50 min range with a ratio of atomic concentrations of Si and Ir close to 0.62/0.38 that corroborates the growth of the $IrSi_{1.6}$ phase. Finally, Fig. 6(c) presents the atomic concentrations depth profile of a sample annealed at 900 °C. Over the first 45 min of sputtering, both the Ir and Si depth profiles indicate that the entire IrSi layer is converted into $IrSi_{1.6}$. Simultaneously, the Ir $4f_{7/2}$ emission line remains centered at 60.8 eV as already observed in experiments conducted in UHV (Fig. 2).

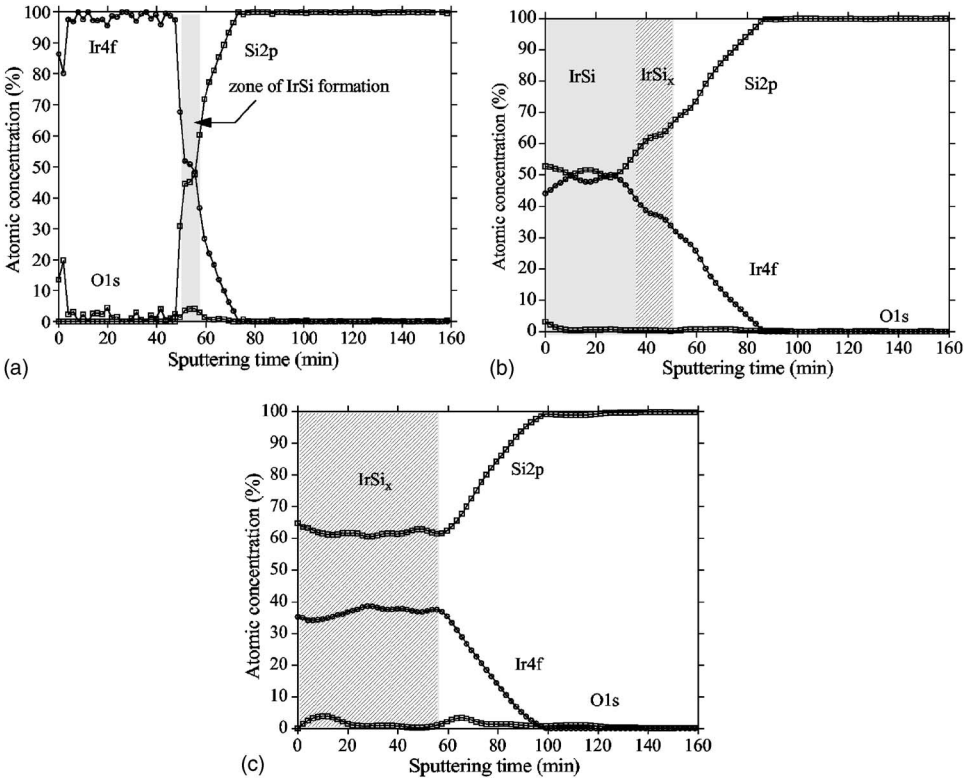

FIG. 6. XPS atomic concentration depth profile obtained from a sample annealed by RTA (a) at 300 °C for 2 min. The shaded zone corresponds to a reacted IrSi phase covered by metallic Ir. (b) At 600 °C for 2 min. The IrSi silicidation reaction is fully completed and the $IrSi_x$ phase starts to grow from the IrSi/Ir interface. (c) At 900 °C for 2 min. The IrSi silicide is fully converted into $IrSi_x$, with x close to 1.6.

IV. TEM CROSS SECTIONS

Transmission electron microscope analyses have been performed on samples covered by a 15 nm thick layer of iridium without or with RTA silicidation (300, 600, and 900 °C for 2 min). Figure 7(a) presents a TEM cross section of the first sample that was not submitted to any thermal budget. The 15 nm iridium layer is clearly identified on a SOI substrate with 100 nm active silicon layer. Although not perfectly uniform, the formation of a ~1 nm thick silicide layer is clearly visible between the metallic iridium and the silicon substrate. Figure 7(b) presents a TEM cross section of a sample annealed at 300 °C for 2 min. The corresponding IrSi layer features (i) a thickness of approximately 3 nm, (ii) grains without particular orientation but with dimensions homogeneously distributed around to the thickness of formed layer as well as (iii) a sharp and uniform silicide/semiconductor interface. Figure 7(c) presents the sample annealed at 600 °C for which the entire Ir layer was consumed by the silicidation reaction. The ~3 nm thick $IrSi_x$ phase that can be distinguished between the top IrSi layer and the silicon substrate confirms results deduced from XPS analysis in Sec. III B 2. Finally, the TEM observation of the sample annealed at 900 °C [Fig. 7(d)] confirms the presence a single silicide phase with very large grains (70 nm) contributing to the roughness of the top surface. Small silicon islands located in the upper part of the silicide layer are also clearly

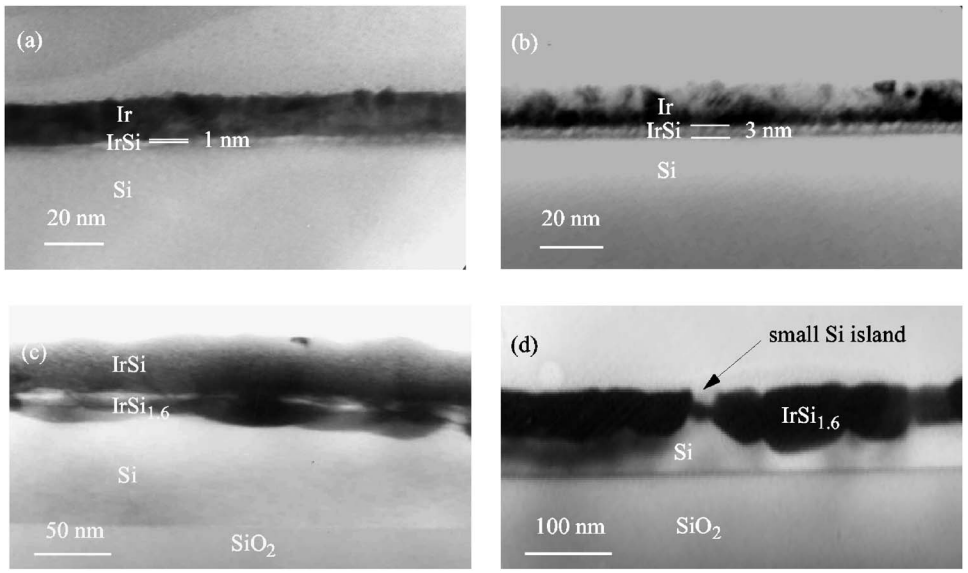

FIG. 7. TEM cross sections of a sample initially covered by a 15+/−1 nm Ir overlayer on a 100 nm thick SOI substrate (a) not annealed, (b) annealed at 300 °C by RTA for 2 min, (c) annealed at 600 °C by RTA for 2 min, and (d) annealed at 900 °C by RTA for 2 min.

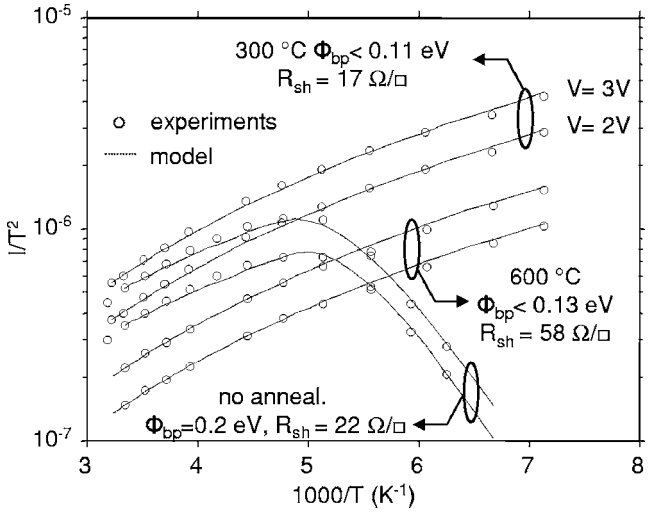

FIG. 8. Experimental Arrhenius plots of back-to-back junctions and calculated characteristics using a transport model that includes thermionic and tunnel emission as well as barrier lowering by image charge induction. The junctions are biased at 2 and 3 V. The three sets of characteristics correspond to iridium silicide contacts obtained at different temperatures (nonannealed or RTA treatments at 300 and 600 °C).

visible. This type of layer morphology further confirms results obtained by Morgan *et al.*[11] who observed a fast diffusion of silicon to the top surface up to 600 °C, which can create Si agglomerates at the silicide grain boundaries. The formation of the $IrSi_3$ phase is not observed.

V. ELECTRICAL MEASUREMENTS

Electrical measurements of iridium silicide contact have been performed to determine annealing conditions that provide the lowest Schottky barrier to holes and, therefore, the lowest specific contact resistance that characterizes the carrier transport through the silicide/silicon interface. Figure 8 presents Arrhenius plots extracted from current voltage characteristics measured at temperatures ranging from 300 to 140 K. The sample with the as deposited Ir layer for which the silicide reaction is not uniform presents a barrier height of 0.2 eV. After RTA activation, it is worth noting that the transition temperature that separates the regime governed by the series resistance, due to the silicon gap between contacts, from the regime driven by the contact resistance could not be determined even for a temperature as low as 140 K. This constitutes an important result that indicates an extremely low contact resistance. Under the above conditions, the extraction scheme predicts a Schottky barrier less than 0.11 eV which corresponds to the lowest detectable figure and worst case value. The Schottky barrier height is below 0.11 eV for the IrSi phase (300 °C) and 0.13 eV for the $IrSi_x$ phase (600 °C). The silicide sheet resistance (R_{sh}) increases slightly at 600 °C, concomitantly with the appearance of the $IrSi_x$ phase. The silicide R_{sh} measured around 17 Ω/□ at 300 °C, increases to 58 Ω/□ at 600 °C. At this temperature, the total series resistance is not only due to the silicon gap between the silicide contacts but is also due to the sheet resistance of the silicide. Because they are affected by different total resistances, the I/T^2 vs $1/T$ characteristics at 300 and 600 °C exhibit the same trend but are shifted from each other. Above 600 °C, R_{sh} increases dramatically (>10 kΩ/□ at 900 °C) due to the degradation of the silicide layer as observed on the TEM cross section. The non uniform morphology of the formed layers precludes the proper extraction of the barrier height.

VI. CONCLUSION

In summary, we have proposed detailed investigations on the formation of iridium silicide obtained using UHV annealing and atmospheric RTA under forming gas. Based on XPS analyses, the stoichiometry of the silicide phases (IrSi, $IrSi_{1.6}$) and the kinetic parameters of IrSi silicidation have been identified. TEM cross sections have provided a cross validation of XPS experiments as far as the morphology and the roughness of the silicide layers are concerned. Finally, electrical characterizations have enabled the identification of the optimum annealing temperature that provides iridium silicide contacts with the lowest Schottky barrier height to holes.

[1] J. Chen, J. P. Colinge, D. Flandre, R. Gillon, J. P. Raskin, and D. Vanhoenacker, J. Electrochem. Soc. **144**, 2437 (1997).
[2] J. A. Lauwers, M. de Potter, O. Chamirian, R. Lindsay, C. Demeurisse, C. Vrancken, and K. Maex, Microelectron. Eng. **64**, 131 (2002).
[3] J. Kittl, J. A. Lauwers, O. Chamirian, M. Van Dal, A. Akheyar, O. Richard, J. Lisoni, M. de Potter, R. Lindsay, and K. Maex, Materials Research Society Symposia Proceedings (Materials Research Society, Warrendale, 2003), Vol. 765, p. 267.
[4] J. Derrien, in *Properties of metal silicides*, edited by K. Maex and M. Van Rossum (IEE INSPEC, London, 1995), p. 164.
[5] SIA Semiconductor Industry Association, "The International Technology Roadmap for Semiconductors-ITRS," 2003.
[6] S. Guha, E. Gusev, M. Copel, L. Ragnarson, and D. Buchanan, MRS Bull. **27**, 226 (2002).
[7] J. Kedzierski, P. Xuan, E. H. Anderson, J. Bokor, T. J. King, and C. Hu, Tech. Dig. - Int. Electron Devices Meet. **2000**, 57.
[8] G. Larrieu and E. Dubois, IEEE Electron Device Lett. **25**, 801 (2004).
[9] M. Jang, Y. Kim, J. Shin, S. Lee, and K. Park, Appl. Phys. Lett. **84**, 741 (2004).
[10] S. P. Murarka, *Silicides for VLSI Applications* (Academic, New York, 1983).
[11] S. J Morgan, R. H. Williams, and J. M. Mooney, Appl. Surf. Sci. **56–58**, 493 (1992).
[12] S. Petersson, J. Baglin, W. Hammer, F. d'Heurle, T. Kuan, I. Ohdomari, J. Pires, and P. Tove, J. Appl. Phys. **50**, 3357 (1979).
[13] I. Ohdomari, T. Kuan and K. Tu, J. Appl. Phys. **50**, 7020 (1979).
[14] K. Hirose, I. Ohdomari, and M. Uda, Phys. Rev. B **37**, 6929 (1988).
[15] M. Wittmer, P. Oelhafen, and K. Tu, Phys. Rev. B **35**, 9073 (1987).
[16] T. Rodríguez, A. Almendra, M. da Silva, J. C. Soares, H. Wolters, A. Rodríguez, and J. Sanz-Maudes, Nucl. Instrum. Methods Phys. Res. B **113**, 279 (1996).
[17] Multipak software manual v. 5.0, Physical electronics.
[18] E. Dubois and G. Larrieu, J. Appl. Phys. **96**, 729 (2004).
[19] G. Larrieu, E. Dubois, X. Wallart, X. Baie, and J. Katcki, J. Appl. Phys. **94**, 7801 (2003).
[20] K. Maex and M. Van Rossum, *Properties of metal silicides*, EMIS Data Reviews Series 14 (INSPEC, London, 1995).
[21] J. C. Fuggle and N. Martensson, J. Electron Spectrosc. Relat. Phenom. **21**, 275 (1980).
[22] A. Almendra, J. Serrano, A. Kling, T. Rodríguez, J. Blanco, M. da Silva, J. Sanz-Maudes, M. Aguilar, and J. C. Soares, Nucl. Instrum. Methods Phys. Res. B **136**, 1040 (1998).